약학석사학위논문

Peptide-coated graphene oxide nanosheets for prolonged blood circulation

펩타이드 수식 그래핀을 이용한 혈중 지속시간 증강연구

2018 년 2 월

서울대학교 약학대학원

약학과 물리약학전공

박 규 태

Abstract

Peptide-coated graphene oxide nanosheets for prolonged blood circulation

Gyuthae Park

Physical Pharmacy, Department of Pharmacy

The Graduate School

Seoul National University

In this study, we modified the surfaces of graphene oxide (GO) nanosheets with a CD47-like signal regulatory protein alpha (SIRP α)-binding peptide (SP). SIRPα is highly expressed in macrophages of the reticuloendothelial system and in tumor-associated macrophages, whereas tumor cells express the surface membrane protein, CD47, which interacts with SIRPα to negatively regulate phagocytosis. The presence of SP on GO nanosheets reduced the macrophage uptake to a greater extent than the PEGylation of such nanosheets. This reduced uptake was found to be mediated by the activation of Src homology region 2 domain-containing phosphatase 1 (SHP-1) and the downstream inhibition of myosin assembly, which is necessary for phagosome formation. Unlike SP-coated GO nanosheets, PEGylated GO nanosheets did not affect myosin assembly or phagocytosis. After *in vivo* systemic administration, the clearance of SP-coated GO nanosheets was slower than that of PEGylated GO nanosheets, and this difference increased with repeated administration. Finally, SP-coated GO nanosheets showed a higher distribution to tumor

tissues than PEGylated GO nanosheets or a physical mixture of SP and GO nanosheets. Our findings indicate that immune-camouflaged GO nanosheets with natural CD47-like SIRPα-binding molecules can reduce the nonspecific loss of such nanosheets through macrophage uptake, thereby enhancing their blood circulation and tumor delivery after multiple injections.

keywords : signal regulatory protein alpha, CD47, macrophage, peptide, graphene nanosheets

Student Number : 2016-21833

Contents

List of Tables

List of Figures

1. Introduction

Graphene-based nanosheets have been widely utilized for photothermal therapy and the delivery of drugs and imaging agents. This reflects the unique features of such sheets, which include their photoresponsiveness, high drug-loading capacity, and surface modifiability (1). However, graphene-based nanosheets are taken up by macrophages of the reticuloendothelial system (RES), limiting their distribution to other tissues following systemic administration. To reduce the uptake of graphene-based nanosheets by macrophages and prolong their circulation in the blood, various approaches have been used to modify the surfaces of nanosheets (2,3).

The introduction of polyethylene glycol (PEG) onto the surfaces of nanosheets is the "gold standard" for such modifications. PEGylation has shown great potential for improving blood residence and enhancing the bioavailability of therapeutics (4). PEG provides graphene nanosheets with a hydrophilic steric hindrance barrier and reduces their clearance by the RES (5). However, the repeated administration of PEGylated formulations can accelerate their clearance from the blood (6). We may therefore need to exploit new, immunologically inspired strategies.

Signal regulatory protein alpha (SIRPα), which is also known as CD171a or Src homology 2 domain-containing protein tyrosine phosphatase substrate-1 (SHPS-1), has drawn considerable attention because it is highly expressed in macrophages of the RES and in tumor-associated macrophages (7,8). The ligand-induced stimulation of SIRPα on the macrophage surface can negatively regulate phagocytosis, and is thus sometimes called a "do not eat me" signal (9). Mechanistically, the stimulation of SIRPα activates Src homology region 2 domain-containing phosphatase 1 (SHP-1). This blocks

myosin assembly, which is essential for phagosome formation. Interestingly, tumor cells do not overexpress SIRPα; instead, they express CD47, which can bind SIRPα to negatively regulate phagocytosis in the tumor microenvironment (10,11).

In this study, we tested whether a CD47-like SIRPα-binding peptide (SP)-coated graphene oxide (GO) nanosheets could decrease their phagocytic uptake by macrophages, as compared to the uptake of PEGylated GO nanosheets. Indeed, we found that this immune-camouflaging strategy can protect GO nanosheets from the phagocytic activity of macrophages, improving their *in vivo* pharmacokinetics and tumor distribution.

2. Materials and methods

2.1. Synthesis of streptavidin-conjugated GO nanosheets

The GO nanosheets were prepared from graphite using Hummer's method, with slight modifications (12). Streptavidin-conjugated GO (SAGO) nanosheets were synthesized by coupling the primary amine groups of streptavidin to the carboxyl groups of GO nanosheets (13). In brief, equimolar amounts (2 mM) of *N*-(3-dimethylaminopropryl-*N*'-ethylcarbodiimine) hydrochloride (Sigma-Aldrich, St. Louis, MO, USA) and *N*-hydroxysulfosuccinimide sodium (Sigma-Aldrich) were combined with GO nanosheets (5 mg in 10 ml of distilled water), and the mixture was stirred for 1 h at room temperature to activate the carboxyl groups of the GO nanosheets. Excess coupling agents and byproducts were removed by dialysis (MWCO 100 K; Spectrum Laboratories, Inc., Rancho Dominguez, CA, USA) against distilled water for 6 h. Recombinant streptavidin (4 mg; ProSpec, East Brunswick, NJ, USA) was added to the activated GO nanosheets, and the mixture was stirred in the dark for 12 h at room temperature. Unreacted free streptavidin was eliminated by dialysis (MWCO 1000 K; Spectrum Laboratories, Inc.) for 24 h. The amount of streptavidin coupled to the GO nanosheets was determined using the bicinchoninic acid (BCA) assay.

2.2. Surface modifications of SAGO nanosheets

The surfaces of the SAGO nanosheets were modified with PEG or SP. To exploit the specific interaction between streptavidin and biotin, we treated SAGO nanosheets with biotinylated PEG (BPEG; MW 2000; Nanocs, New York, NY, USA) or biotinylated SP (BSP; biotin-GNYTCEVTELTREGETIIELK; Peptron, Daejeon, Republic of Korea) (14). In brief, 20 μl of 1 mM BPEG or BSP in 1 ml of

dimethyl sulfoxide was mixed with 0.5 mg of SAGO nanosheets for 1 h at room temperature. The BPEG-modified SAGO (BPEG-SAGO) and BSP-modified SAGO (BSP-SAGO) nanosheets were collected by centrifugation at 1600 × *g* for 30 min in an Amicon Ultra centrifugal filter (MWCO 100 K). Where indicated, the SAGO nanosheets (1 mg) were incubated for 1 h with 0.4 mg of distearoylphosphatidyl ethanolamine (DSPE)-PEG_{5000}-Alexa Fluor 680 to fluorescently label the GO. The nanosheets were collected using an Amicon Ultra centrifugal filter (MWCO 100 K), and their fluorescence intensity was measured with a multiplate reader (Gemini XS; Molecular Devices, Sunnyvale, CA, USA). A physical mixture of free SP and SAGO nanosheets was prepared as a control.

2.3. Characterization of nanosheets

The morphologies of GO, SAGO, and BSP-SAGO nanosheets were examined by transmission electron microscopy (TEM). Nanosheet samples were dried on a Lacey SiO TEM grid (TED Pella, Redding, CA, USA) and observed using TEM (JEM-2100F, JEOL Ltd, Tokyo, Japan). The elemental contents of various nanosheets were measured using quantitative scanning TEM-energy dispersive spectroscopy (STEM-EDS) mapping and analysis (15,16). Thickness was measured using atomic force microscopy (AFM) (XE-100; Park Systems, Suwon, Republic of Korea) in non-contact mode, as previously described (17).

2.4. Cell differentiation

Human THP-1 monocyte cells (Korea Cell Line Bank, Seoul, Republic of Korea) were maintained in RPMI-1640 supplemented with 10% heat-inactivated FBS (Gibco-BRL Life Technologies, Carlsbad,

CA, USA), 100 units per ml penicillin, and 100 mg ml^{-1} streptomycin at 37 °C in a humidified 5% CO2 incubator. Before each experiment, the THP-1 cells were incubated for 48 h with 100 ng ml^{-1} phorbol myristate acetate (PMA; Sigma-Aldrich) to induce their differentiation into macrophage-like cells (18). This differentiation was confirmed by morphological observation of adherent cells under an optical microscope (Leica DM IL, Wetzlar, Germany).

2.5. Immunostaining of surface-expressed SIRPα

THP-1 cells (1×10^5 cells per ml) were fixed with 4% paraform-aldehyde, blocked at 4 °C for 30min with 3% bovine serum albumin (BSA) in phosphate-buffered saline (PBS), and then incubated for 1 h at room temperature with a phycoerythrin (PE)-conjugated antihuman SIRPα antibody (diluted 1 : 50; BD Bioscience, San Jose, CA, USA). Cellular fluorescence was observed under an LSM 710 laser-scanning confocal microscope (Carl Zeiss, Jena, Germany). The cells were then washed, stained with the PE-conjugated anti-human SIRPα antibody (BD Bioscience), and analyzed using a BD FACSCalibur equipped with Cell Quest Pro software (BD Bioscience).

In some experiments, SCC7 cells (2×10^5 cells) were stained with the PE-conjugated anti-human SIRPα antibody (BD Bioscience), and analysed using a BD FACSCalibur equipped with Cell Quest Pro software (BD Bioscience).

2.6. Cellular uptake measurements

The cellular uptake of surface-modified GO nanosheets was assessed by measuring the fluorescence intensity of cells treated with fluorescent-lipid-labeled nanosheets. PMA-activated THP-1 cells and murine squamous cell carcinoma SCC7 cells were seeded onto cover

glasses in a 24-well plate (2×10^5 cells per well), and then treated for 1 h with 20 μg per well of PEG-SAGO or BSP-SAGO nanosheets labeled with DSPE-PEG_{5000}-Alexa Fluor 680. The cells were washed, fixed with 4% paraformaldehyde, stained with 2 μg ml^{-1} Hoechst 33258 (Sigma-Aldrich) for 10 min, and observed under an LSM 710 laser-scanning confocal microscope (Carl Zeiss). In some experiments, THP-1 cells were seeded onto cover glasses in a 24-well plate (2×10^5 cells per well) and left untreated or treated for 1 h with 20 μg of various nanosheets. The cells were then washed, stained with the PE-conjugated anti-human SIRPα antibody (BD Bioscience), and analysed using a BD FACSCalibur equipped with Cell Quest Pro software (BD Bioscience).

2.7. SIRPα-binding affinity measurement

The SIRPα-binding affinity of nanosheets was determined using a microscale thermophoresis technique (19). Serial dilutions of THP-1 cell lysates in HEPES-buffered saline containing 0.05% Tween-20 were mixed with nanosheets that had been fluorescently labeled with DSPE-PEG_{5000}-Alexa Fluor 680 (18). The amount of SIRPα in THP-1 cell lysates was analyzed using a human SIRPα enzyme-linked immunosorbent assay (ELISA) kit (MyBioSource Inc., San Diego, CA, USA). The thermophoretic movement of fluorescently labeled molecules was measured using a Monolith NT.115 MST instrument (NanoTemper, Munich, Germany). Binding curves and K_d values were calculated using the NT analyzer software (Nano Temper).

2.8. Monitoring inhibition of myosin assembly

The interruption of myosin IIA assembly in phagocytic signaling by functionalized GO nanosheets was tested using NSC-87877 (Tocris

Bioscience, Bristol, UK), a specific inhibitor of SHP-1 (20). THP-1 cells seeded to 24-well plates (2×10^5 cells per well) were treated with 20 μg per well of BSP-SAGO nanosheets for 1 h. The cells were fixed, permeabilized with 0.1% Triton X-100, stained with 2 μg ml^{-1} Hoechst 33258 (Sigma-Aldrich) for 10 min, blocked with 5% BSA in PBS for 1 h, incubated with the anti-MHY9 (non-muscle myosin IIA) primary antibody (Sigma-Aldrich), and then incubated with a fluorescently labeled rabbit IgG secondary antibody (BioLegend, San Diego, CA, USA). MHY9 immunofluorescence was observed under an LSM 710 laser-scanning confocal microscope (Carl Zeiss).

2.9. Animals

In vivo experiments were conducted using 5-wk-old female Balb/c and athymic nude mice supplied by Raon Bio (Yongin, Gyeonggi-do, Republic of Korea). Animals were raised under standard pathogen-free conditions at the Animal Center for Pharmaceutical Research, Seoul National University. All animal experiments were conducted in accordance with the Guidelines for the Care and Use of Laboratory Animals of the Institute of Laboratory Animal Resources, Seoul National University (approved animal experimental protocol number, SNU-150609-2-1).

2.10. Quantification of GO nanosheets in serum

Female Balb/c mice were administered with BPEG-SAGO nanosheets, a physical mixture of SP and SAGO nanosheets, or BSP-SAGO nanosheets (all at a nanosheet dose of 1 mg kg^{-1}), and blood was sampled at the indicated time points post-injection. For multiple injections, three injections were given at 7 day intervals and

blood was sampled at the indicated time points after the final injection. The serum levels of the SAGO nanosheets were detected using ELISA. Briefly, 96-well plates (SPL, Suwon, Republic of Korea) were coated with 2 μg ml^{-1} capture antibody, incubated overnight at 4 °C, blocked with 2% (w/v) BSA for 2 h at 37 °C, and washed three times with PBS containing 0.1% Tween-20 (PBS-T). Mouse serum (diluted 1 : 50) was added, the plates were incubated for 2 h at room temperature, the unbound antibody was removed, a peroxidase conjugated detection antibody (1 : 5000) was added, and the plates were incubated for 1 h at 37 °C. The plates were washed with PBS-T, a 3,3',5,5'-tetramethyl benzidine substrate solution (Pierce, Rockford, IL, USA) was added, and the plates were incubated for 10 min. The peroxidase-based colorimetric reaction was stopped by the addition of 0.5 M sulfuric acid (H_2SO_4, Sigma-Aldrich), and absorbance was measured at 450 nm using an ELISA plate reader (Sunrise-Basic TECAN, Männedorf, Switzerland).

2.11. Pharmacokinetic analysis

Pharmacokinetic analyses were performed using the previously described non-compartmental model (21). The mean residence time (MRT) was calculated by dividing the area under the curve (AUC) by the area under the momentum curve (AUMC). Pharmacokinetic parameters were calculated using the WinNonlin software (Scientific Consulting Inc., Lexington, KY, USA).

2.12. *In vivo* molecular imaging

The *in vivo* tumor distributions of various functionalized nanosheets were examined by molecular imaging. Female 5-wk-old athymic nude mice were subcutaneously inoculated in the left dorsal side with 1 ×

10^6 murine squamous cell carcinoma SCC7 cells, and tumors were allowed to grow over time. After the SCC7-cell-derived tumor volumes reached ~150 mm^3, the mice were intravenously administered nanosheets labeled with DSPE-PEG_{5000}-Alexa Fluor 680 at a fluorescent lipid dose of 10 nM per mouse. At the indicated time points post-dose, the tumor tissue distribution of fluorescent nanosheets was assessed using an eXplore Optix System (Advanced Research Technologies, Inc., Montreal, Canada) with a 670 nm filter set.

2.13. Statistics

Experimental data were statistically evaluated by two-tailed analysis of variance (ANOVA) using the Student-Newman-Keuls test as a *post hoc* test. All statistical analyses were performed using the SigmaStat software (version 3.5; Systat Software, Richmond, CA, USA). A P-value < 0.05 was considered significant.

3. Results

3.1. Design and characterization of nanosheets

The surfaces of SAGO nanosheets were modified with BSP through non-covalent streptavidin-biotin interactions (Fig. 1A). The specific interaction between streptavidin and the biotin moiety of BSP should prevent the nonspecific-conjugation-induced alteration of the peptide's three-dimensional configuration.

Elemental mapping analyses revealed that nitrogen, which we detected as a proxy for SA, was present on the SAGO and BSP-SAGO nanosheets, but not on plain GO nanosheets (Fig. 1B).

The thickness of the GO nanosheets was slightly increased by conjugation with SA (Fig. 1C). The further modification of SAGO with BPEG or BSP increased the nanosheet thickness, but there was a lack of substantial difference in thickness between the BPEG- and BSP-modified nanosheets (Fig. 1C).

3.2. Immune cell-specific regulation of BSP-SAGO

We propose a model for the immune cell-specific regulation of phagocytosis by BSP-SAGO nanosheets (Fig. 2). BPEG-SAGO nanosheets show little specific interaction with SIRPα on immune cells, and their cellular uptake by macrophages is not affected by SHP-1 signaling (Fig. 2A). In contrast, the binding of the SP moiety of BSP-SAGO nanosheets to SIRPα on immune cells activates SHP-1 signaling, which inhibits the myosin assembly required for phagosome formation, and thus negatively regulates phagocytosis (Fig. 2B). Unlike macrophages, tumor cells lack SIRPα and express CD47. Thus, the phagocytosis of BSP-SAGO nanosheets by tumor cells is not negatively regulated (Fig. 2C).

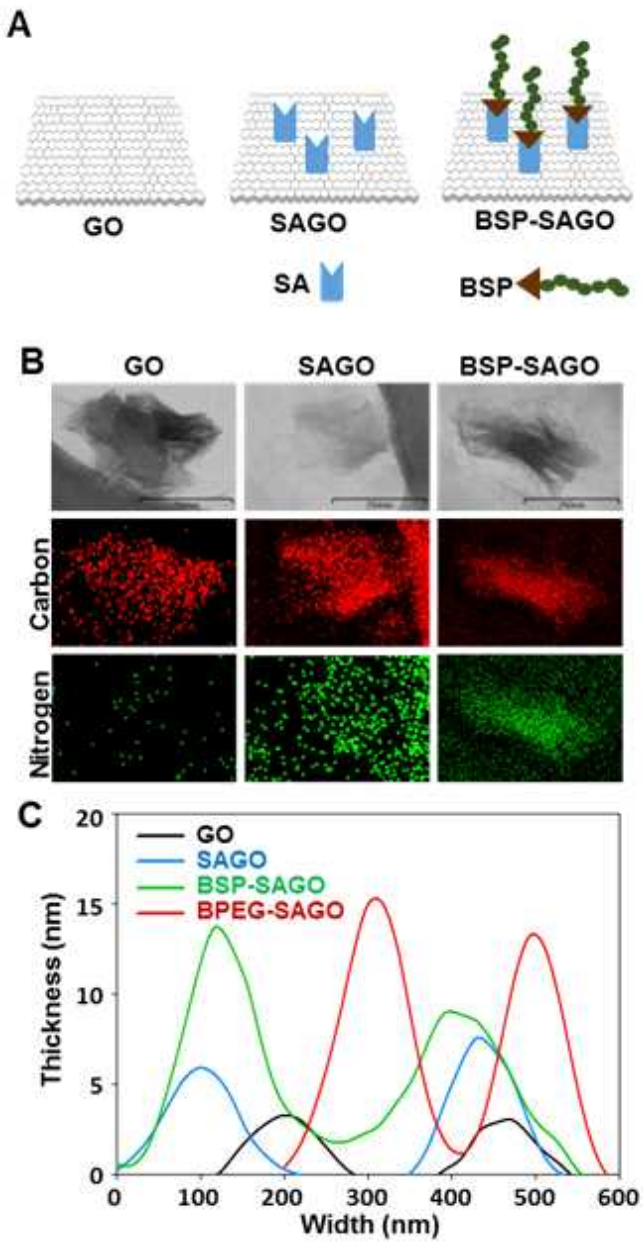

Figure 1. Characterization of nanosheets.
(A) Schematic illustrations of GO, SAGO, BSP-SAGO nanosheets. (B) STEM-EDS mapping images of GO, SAGO, and BSP-SAGO nanosheets. Elemental mapping images of carbon and nitrogen are pseudocolored red and green, respectively. (C) The thicknesses of the various nanosheets were measured using AFM.

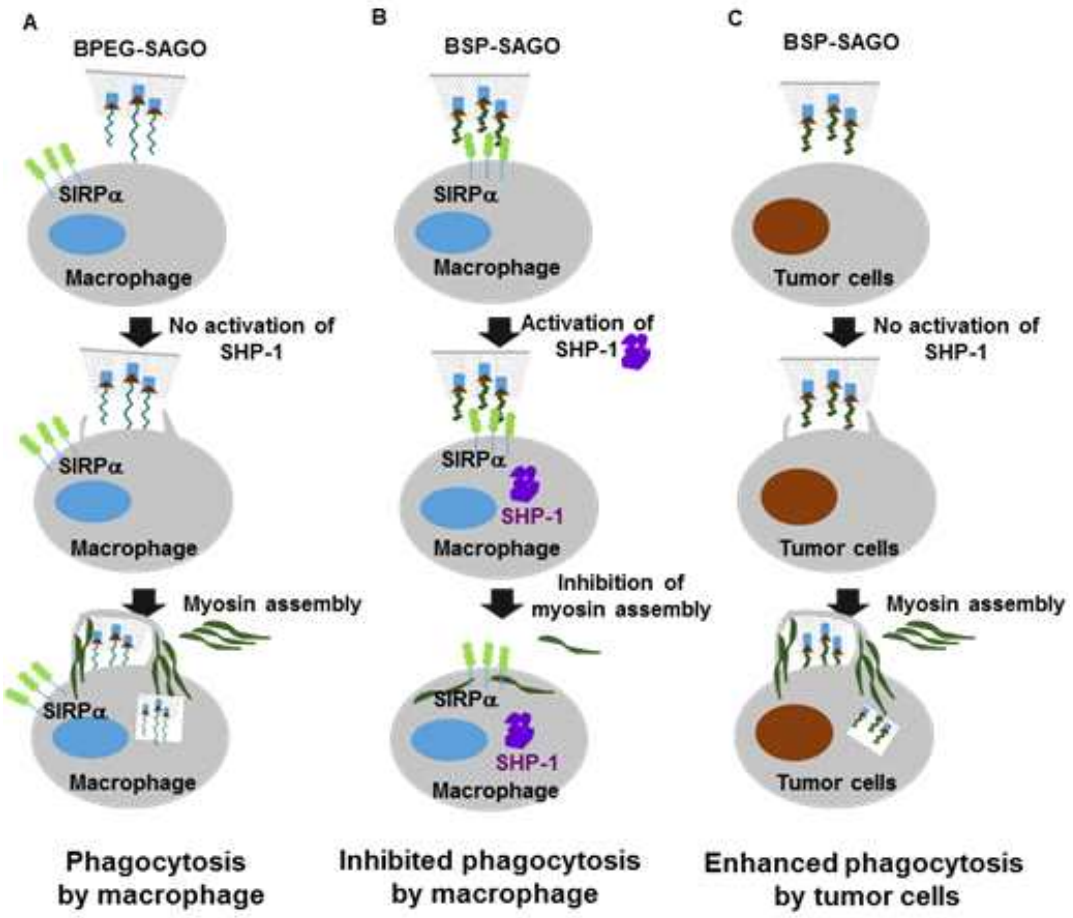

Figure 2. Schematic illustration of uptake of nanosheets by immune cells or tumor cells. The BPEG-SAGO uptake pathway in macrophages (A), the decreased uptake of BSP-SAGO by macrophages (B), and the increased uptake of BSP-SAGO in tumor cells (C) are illustrated. (A) The nonspecific binding of BPEG-SAGO nanosheets to macrophages triggers myosin assembly and the engulfment of nanosheets through phagosome formation. (B) The specific binding of BSP-SAGO nanosheets to SIRPα on macrophages inhibits myosin assembly (which is needed to form phagosomes) by activation of SHP-1 signaling, and exerts antiphagocytic activity. (C) The nonspecific binding of BSP-SAGO nanosheets to tumor cells which lack SIRPα triggers myosin assembly and the phagocytosis of nanosheets.

3.3. Uptake of nanosheets by SIRPα-expressing immune cells

We hypothesized that the surface-modification of nanosheets with SP would reduce their SIRPα-mediated uptake by immune cells. We used immunofluorescence staining with an anti-SIRPα antibody to confirm that SIRPα was expressed on the surfaces of our PMA-differentiated THP-1 macrophage-like cells (Fig. 3B). We then treated these THP-1 cells with fluorescent lipid-labeled nanosheets and performed fluorescence microscopy. We observed that the fluorescent lipid-labeled BPEG-SAGO nanosheets were clearly taken up (Fig. 3C), whereas the BSP-SAGO nanosheets showed little uptake by THP-1 cells (Fig. 3D).

Little differences in the cellular uptake patterns between BPEG-SAGO (Fig. 3E) and BSP-SAGO (Fig. 3F) may be due to the lack of SIRPα expression on SCC7 cells (Fig. 3J).

3.4. SIRPα-binding affinity of nanosheets

To test whether the differences in the cellular uptake of nanosheets could be attributed to the interaction with SIRPα, we measured the binding affinity of BPEG-SAGO and BSP-SAGO nanosheets for SIRP α using the microscale thermophoresis technique. As shown in Fig. 4, we found that while the BPEG-SAGO nanosheets (Fig. 4A) bound SIRPα with low affinity, the BSP-SAGO nanosheets (Fig. 4B) bound strongly to SIRPα, with a nanomolar K_d value of 90.0 ± 26.1 nM.

3.5. SHP-1-mediated antiphagocytic activity upon SIRPα binding

After BSP-SAGO nanosheets bind to cell-surface-displayed SIRPα, their uptake was prevented by SIRPα-mediated inhibitory signals. we tested whether the binding of BSP-SAGO nanosheets to SIRPα on THP-1 cells affected the SHP-1-activation-dependent assembly of the

myosin cytoskeleton. In the absence of a specific SHP-1 inhibitor, NSC-87877 (20), there was no notable cellular uptake of fluorescent lipid-labeled BSP-SAGO nanosheets, and myosin staining was dispersed at various points within the cells (Fig. 5A). In contrast, the NSC-87877-induced inhibition of SHP-1 strongly increased the assembly of myosin and the cellular delivery of BSP-SAGO nanosheets (Fig. 5B).

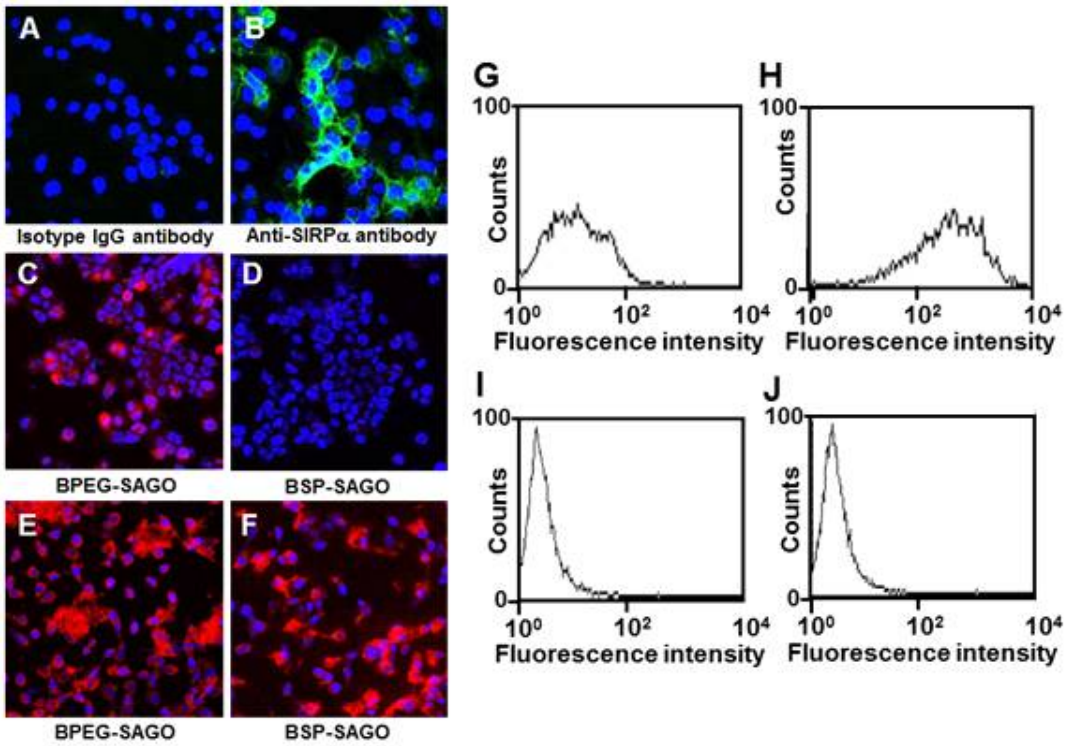

Figure 3. Uptake of nanosheets by immune cells and cancer cells. PMA-treated THP-1 cells were immunostained with fluorescence labeled IgG isotype control antibody (A) or anti-SIRPα antibody (B), and nuclei were counterstained with Hoechst 33258 (blue). Activated THP-1 cells (C and D) and SCC7 cells (E and F) were treated with Alexa Fluor-680 lipid derivative-labeled BPEG-SAGO (C and E) or BSP-SAGO (D and F) nanosheets. Cell nuclei were counterstained with Hoechst 33258 (blue). The uptake of Alexa Fluor 680 lipid-labeled nanosheets was observed using confocal microscopy and is shown as merged images. Activated THP-1 cells were unstained (G) or immunostained with anti-SIRPα antibody for untreated cells (H). SCC7 cells were unstained (I) or immunostained with anti-SIRPα antibody (J).

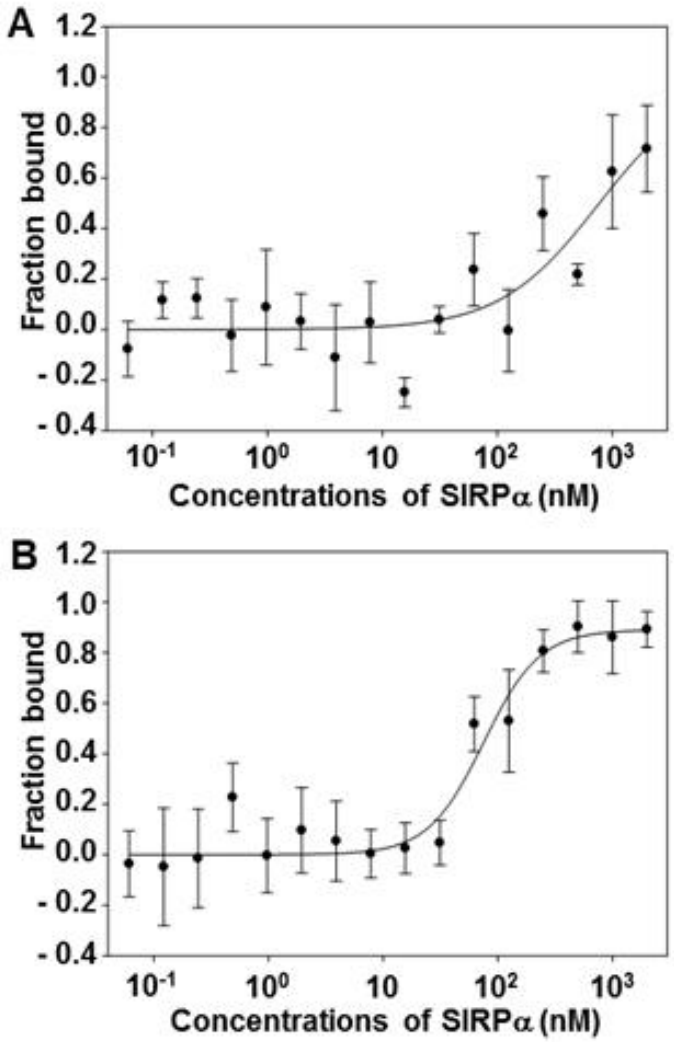

Figure 4. SIRPα-binding affinity of nanosheets.
Serial dilutions of SIRPα mixed with fluorescent marker-labeled BPEG-SAGO (A) or BSP-SAGO (B) The binding affinity was evaluated using microscale thermophoresis (19).

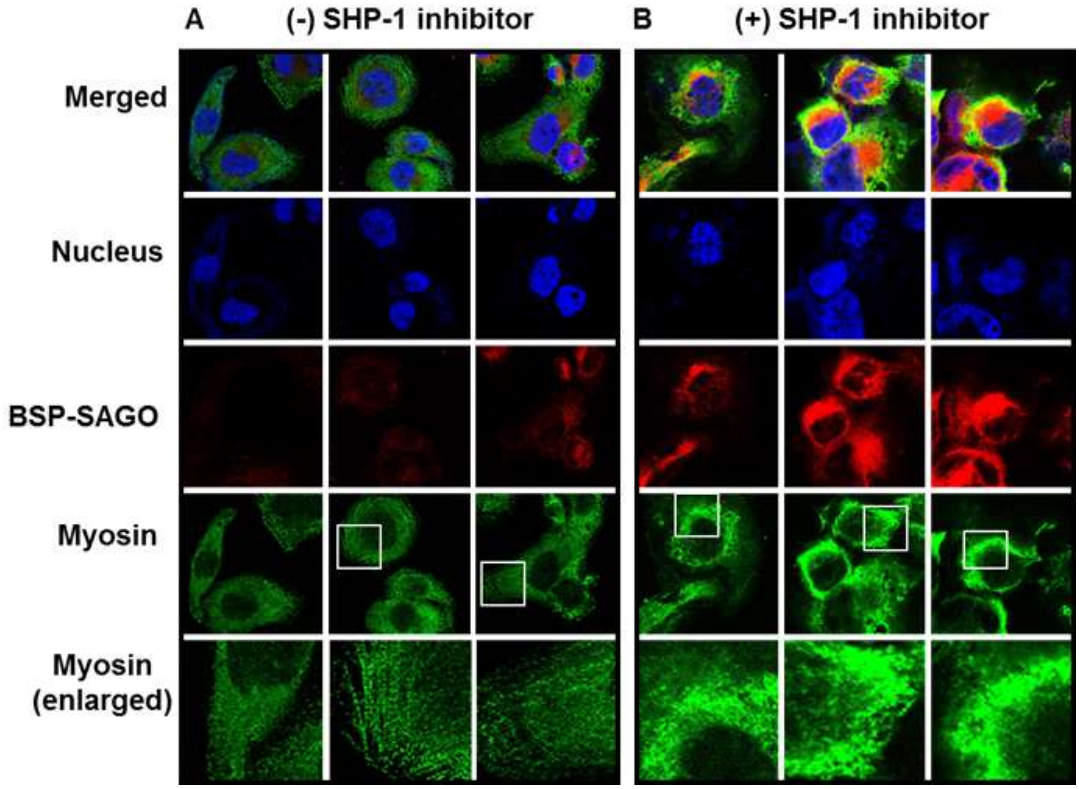

Figure 5. Role of SHP-1 in myosin assembly and phagocytosis of BSP-SAGO. THP-1 cells were left untreated (A) or pretreated with the SHP-1 inhibitor, NSC-87877 (B). Nuclei were stained with Hoechst 33258, and the cellular uptake of Alexa Fluor 680 lipid-labeled BSP-SAGO nanosheets was visualized using confocal microscopy. Myosin assembly was detected using immunostaining with a fluorescent anti-myosin antibody. Fluorescence images were obtained from three random fields for each group.

3.6. *In vivo* pharmacokinetics of BSP-SAGO nanosheets

We tested whether the ability of BSP-SAGO nanosheets to inhibit phagocytosis could affect their blood circulation time following systemic administration. Eight hours after the first injection, the blood levels of BSP-SAGO nanosheets were 2.5-fold higher than those of BPEG-SAGO nanosheets (Fig. 6A). The AUC and AUMC values after the first injection of BSP-SAGO nanosheets were 4.0- and 9.3-fold higher, respectively, than those of BPEG-SAGO nanosheets (Table 1). The MRT value obtained after the first injection of BSP-SAGO nanosheets was 2.3-fold higher than that of BPEG-SAGO nanosheets.

These pharmacokinetic parameters changed with multiple injections of each nanosheet. Relatively minimal changes were seen for the BSP-SAGO nanosheets, but larger changes were seen for the BPEG-SAGO nanosheets. After the second and third injections, the MRT values of the BSP-SAGO nanosheets were 4.7- and 4.4-fold greater, respectively, than those of the BPEG-SAGO nanosheets (Fig. 6B).

The physical mixture of SP and SAGO nanosheets showed prolonged circulation compared with the BPEG-SAGO nanosheets, although the difference was not as pronounced as that seen for the BSP-SAGO nanosheets.

3.7. Tumor accumulation of BSP-SAGO nanosheets

In SCC7 tumor-bearing mice *in vivo*, the BSP-SAGO nanosheets showed enhanced tumor distribution compared with the BPEG-SAGO nanosheets and the physical mixture of SP and SAGO nanosheets (Fig. 7). At 8 h after intravenous injection into SCC7 tumor-bearing mice, the tumor tissue accumulation of the BSP-SAGO nanosheets

was 2.3- and 2.0-fold greater than those of the BPEG-SAGO nanosheets and the physical mixture of SP and SAGO nanosheets, respectively. This greater tumor distribution of the BSP-SAGO nanosheets compared with other nanosheet formulations was maintained for over 48 h.

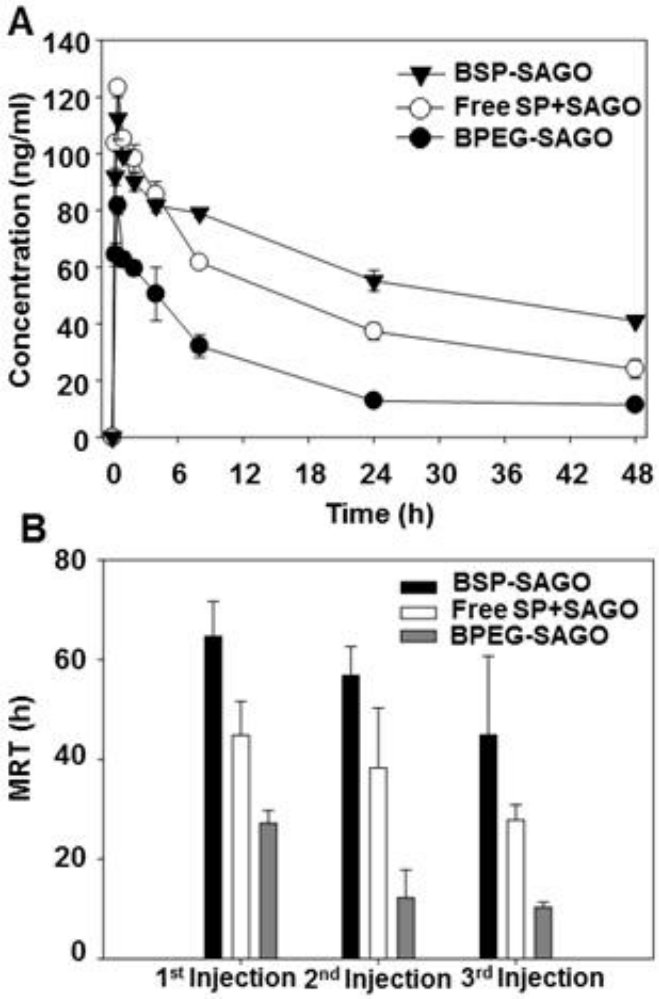

Figure 6. Pharmacokinetics of nanosheets after intravenous injection. Balb/c mice were intravenously injected with BPEG-SAGO nanosheets, a physical mixture of SP and SAGO nanosheets or BSP-SAGO nanosheets. Blood samples were collected at various time points. (A) Blood concentrations of nanosheets after the first intravenous injection. (B) Mice were injected three times at 1-week intervals. The MRT values of the repeated injections are compared for the various nanosheets.

Table 1.
Pharmacokinetic parameters of administered nanosheets.

		PEG-SAGO	Free SP + SAGO	SP–SAGO
AUC (ng h ml^{-1})	1st	1405.6 ± 30.2	3325.7 ± 317.7	5584.2 ± 351.8
	2nd	934.1 ± 94.6	2944.8 ± 541.2	4046.8 ± 269.2
	3rd	766.9 ± 21.4	2598.1 ± 122.5	3689.0 ± 774.0
AUMC (ng h^2 ml^{-1})	1st	38962.8 ± 4274.3	150529.6 ± 35489.2	362635.2 ± 60970.5
	2nd	11420.7 ± 6154.0	117175.9 ± 52204.7	230413.4 ± 36426.6
	3rd	7896.9 ± 669.6	72442.3 ± 9332.2	173727.3 ± 66847.3
MRT (h)	1st	27.7 ± 2.5	44.8 ± 6.8	64.7 ± 7.0
	2nd	12.0 ± 5.6	38.3 ± 12.0	56.8 ± 5.8
	3rd	10.3 ± 1.0	27.8 ± 3.1	44.9 ± 15.8
Cl (ml h^{-1})	1st	7.1 ± 0.2	3.0 ± 0.3	1.8 ± 0.1
	2nd	10.8 ± 1.1	3.5 ± 0.7	2.5 ± 0.2
	3rd	13.0 ± 0.4	3.9 ± 0.2	2.8 ± 0.6
Vd (ml)	1st	186.7 ± 18.6	143.3 ± 7.3	116.4 ± 7.6
	2nd	106.4 ± 59.0	130.7 ± 21.6	139.0 ± 14.6
	3rd	186.4 ± 37.3	106.5 ± 4.3	120.2 ± 20.0

AUC: area under the curve, AUMC: area under the momentum curve, MRT: mean residence time. Cl: clearance, Vd: volume of distribution.

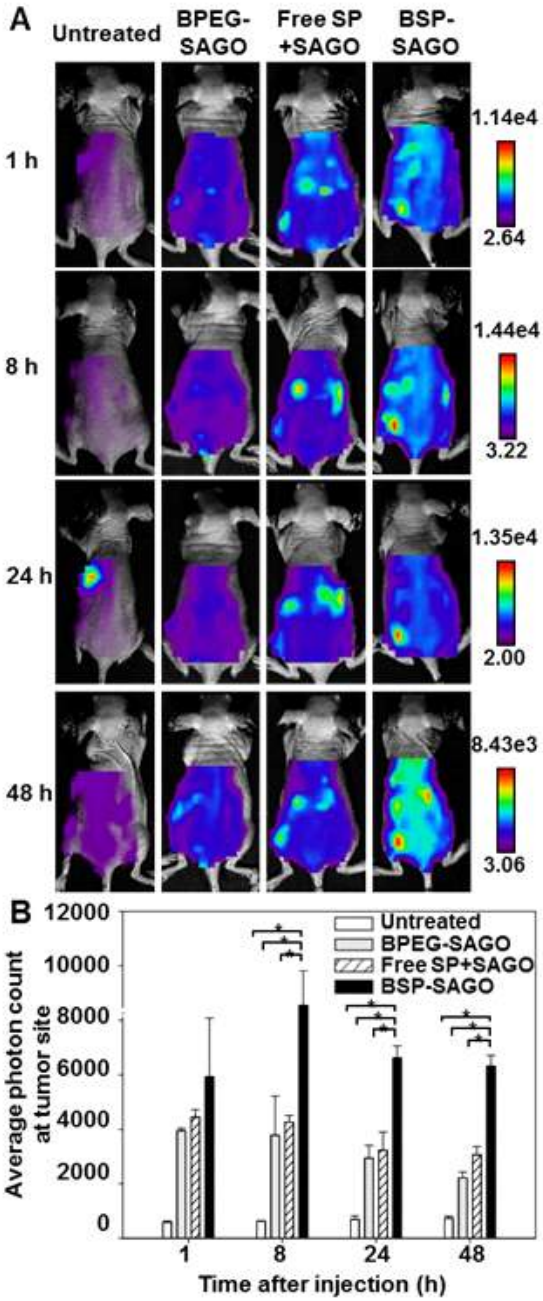

Figure 7. Tumor distribution of nanosheets in tumor-bearing mice. SCC7 tumor-bearing mice were intravenously injected with BPEG-SAGO nanosheets, a physical mixture of SP and SAGO nanosheets, or BSP-SAGO nanosheets (all fluorescent lipid-labeled). The tumor distribution of nanosheets was visualized using molecular imaging (A). Photon counts at the SCC7 tumor site were analyzed using the Optiview program (B). $*P < 0.05$.

4. Discussion

In this study, we demonstrated that BSP-SAGO nanosheets showed improved blood circulation and tumor accumulation time as compared to BPEG-SAGO nanosheets and physical mixture of SP and SAGO nanosheets by negatively regulating the phagocytosis of macrophages.

BSP- and BPEG-SAGO nanosheets were prepared by using streptavidin to non-covalently anchor BSP and BPEG on GO nanosheets, respectively. Streptavidin, which binds biotin with high affinity and specificity, has been used for the surface functionalization of nanomaterials (13). The specific interaction between streptavidin and the biotin moiety of BSP should prevent the non specific-conjugation-induced alteration of the peptide's three-dimensional configuration. Moreover, the specific interaction-based anchoring allowed us to use a simple physical mixing process rather than needing to apply catalysts and a multistep chemical conjugation process. Results of elemental mapping and AFM imaging revealed formation of the nanosheets.

We observed that the fluorescent lipid-labeled BPEG-SAGO nanosheets were clearly taken up whereas the BSP-SAGO nanosheets showed little uptake by PMA-activated THP-1 cells. Thus, our results indicate that SP was more effective than PEG in reducing nonspecific interactions with SIRPα-expressing THP-1 immune-like cells. We chose PEG for comparison because it is known to decrease the interaction of nanoparticles with cell membranes, and has been widely used to modify the surfaces of graphene-based nanosheets (22) and liposomes (23) to enable them to evade phagocytosis. However, as shown in Fig. 3C, the PEGylated nanosheets underwent active phagocytosis in our THP-1 cells. Our observations are consistent with previous reports that PEGylated graphene nanosheets

undergo phagocytosis and trigger the production of proinflammatory cytokines in macrophages (24,25). Additionally, PEGylation decreases the cellular uptake through a hydrophilic polyethylene glycol-clouding effect, and thus shows little cell specificity. This lack of cell specificity means that PEGylated systems show reduced delivery to both the RES and target tissues, such as tumor cells. This phenomenon has been termed the "PEG dilemma" (26,27).

Given that SHP-1 critically contributes to the inhibition of phagocytosis by suppressing myosin assembly which is required for phagosome formation in macrophages (28,29), our observations support the notion that the uptake of BSP-SAGO nanosheets is inhibited by the activation of SHP-1 and subsequent blockade of myosin assembly upon SIRPα binding. Here, we found that NSC-87877 activates immune cell phagocytosis of BSP-SAGO. Thus, we speculate that the co-delivery of active substances such as vaccine antigens (30,31) together with SHP-1 inhibitors could promote their uptake into immune cells.

In vivo pharmacokinetics of nanosheets showed that compared to BPEG-SAGO nanosheets and the physical mixture of SP and SAGO, BSP-SAGO nanosheets exhibited prolonged blood circulation. After the multiple injections, the MRT values of the BSP-SAGO nanosheets were more than 4-fold higher than those of the BPEG-SAGO nanosheets. We speculate that this difference might reflect the induction of antibodies against PEG molecules, as previous studies found that the clearance of PEGylated therapeutics was increased upon repeated injections (6), and that repeated administration of PEGylated proteins (32,33) or PEGylated liposomes (34) could induce PEG-specific antibodies.

Additional studies are needed to examine a phenomenon that the

physical mixture of SP and SAGO nanosheets also showed prolonged circulation compared with the BPEG-SAGO nanosheets. However, we previously reported that another peptide containing six phenylalanine residues can adsorb onto reduced GO nanosheets through $\pi-\pi$ interactions (18). Thus, we cannot exclude the possibility that the increased circulation of the physical mixture could reflect the spontaneous nonspecific physical adsorption of SP onto the SAGO nanosheets.

The greater tumor distribution of the BSP-SAGO nanosheets in SCC7 tumor-bearing mice might be explained by their prolonged circulation in the blood. Several groups have reported that an increase in the blood circulation time of a nanomaterial can increase its tumor distribution (35,36). Moreover, our group previously reported that functionalization with amphiphilic poloxamer 407 increased the circulation time and tumor distribution of graphene nanosheets (22).

The enhanced tumor distribution could also reflect the preferential uptake of the BSP-SAGO nanosheets by tumor cells compared with macrophages. Recent studies have shown that tumor-associated macrophages express SIRPα, whereas the tumor cells themselves express CD47, which inhibits phagocytosis by macrophages (37,38). The decreased phagocytosis of the BSP-SAGO nanosheets by tumor-associated macrophages may increase the blood circulation time and their uptake by tumor cells.

5. Conclusion

We herein demonstrate that SP tethered to GO nanosheets negatively regulates their phagocytosis by macrophages via activating SHP-1 and inhibiting myosin assembly. This negative regulation of phagocytosis was uniquely observed for BSP-SAGO nanosheets, not for PEGylated GO nanosheets. Moreover, we observed that repeated dosing with BSP-SAGO nanosheets provided prolonged blood circulation and enhanced tumor accumulation compared with repeatedly administered BPEG-SAGO nanosheets. Although GO nanosheets were used for surface modification in this study, surface coating with SP can be extended to other carbon-based nanostructures. Moreover, our findings suggest that BSP-SAGO nanosheets may be applicable for the tumor-tissue delivery of anticancer drugs and imaging agents.

6. References

1. G. Shim, M. G. Kim, J. Y. Park and Y. K. Oh, Graphene-based nanosheets for delivery of chemotherapeutics and biological drugs, Adv. Drug Delivery Rev., 2016, 105, 205-227.

2. W. Miao, G. Shim, C. M. Kang, S. Lee, Y. S. Choe, H. G. Choi and Y. K. Oh, Cholesteryl hyaluronic acid-coated, reduced graphene oxide nanosheets for anti-cancer drug delivery, Biomaterials, 2013, 34, 9638-9647.

3. G. Shim, J. Y. Kim, J. Han, S. W. Chung, S. Lee, Y. Byun and Y. K. Oh, Reduced graphene oxide nanosheets coated with an anti-angiogenic anticancer low-molecular-weight heparin derivative for delivery of anticancer drugs, J. Controlled Release, 2014, 189, 80-89.

4. K. Yang, J. Wan, S. Zhang, Y. Zhang, S. T. Lee and Z. Liu, In vivo pharmacokinetics, long-term biodistribution, and toxicology of pegylated graphene in mice, ACS Nano, 2010, 5, 516-522.

5. M. Xu, et al., Improved in vitro and in vivo biocompatibility of graphene oxide through surface modification: poly (acrylic acid)-functionalization is superior to pegylation, ACS Nano, 2016, 10, 3267-3281.

6. A. Lila, S. Abu, H. Kiwada and T. Ishida, The accelerated blood clearance (Abc) phenomenon: clinical challenge and approaches to manage, J. Controlled Release, 2013, 172, 38-47.

7. Y. F. Pan, Y. X. Tan, M. Wang, J. Zhang, B. Zhang, C. Yang, Z. W. Ding, L. W. Dong and H. Y. Wang, 2013 Signal regulatory protein α is associated with tumor-polarized macrophages phenotype switch and plays a pivotal role in tumor progression, Hepatology, 2013, 58, 680-691.

8. A. N. Barclay and T. K. Van den Berg, The interaction between signal regulatory protein alpha (SIRPα) and CD47: structure, function, and therapeutic target, Annu. Rev. Immunol., 2014, 32, 25-50.

9. Y. Murata, T. Kotani, H. Ohnishi and T. Matozaki, The CD47-SIRPa signalling system: its physiological roles and therapeutic application, J. Biochem., 2014, 155, 335-344.

10. T. Matozaki, Y. Murata, H. Okazawa and H. Ohnishi, Functions and molecular mechanisms of the CD47-SIRP alpha signalling pathway, Trends Cell Biol., 2009, 19, 72-80.

11. E. Sick, A. Jeanne, C. Schneider, S. Dedieu, K. Takeda and L. Martiny, CD47 update: a multifaceted actor in the tumour microenvironment of potential therapeutic interest, Br. J. Pharmacol., 2012, 167, 1415-1430.

12. W. Miao, G. Shim, G. Kim, S. Lee, H. J. Lee, Y. B. Kim, Y. Byun and Y. K. Oh, Image-guided synergistic photothermal therapy using photoresponsive imaging agent-loaded graphene-based nanosheets, J. Controlled Release, 2015, 211, 28-36.

13. B. J. Hong, O. C. Compton, Z. An, I. Eryazici and S. T. Nguyen, Successful stabilization of graphene oxide in electrolyte solutions: enhancement of biofunctionalization and cellular uptake, ACS Nano, 2012, 6, 63-73.

14. P. L. Rodriguez, T. Harada, D. A. Christian, D. A. Pantan, R. K. Tsai and D. E. Discher, Minimal self peptides that inhibit phagocytic clearance and enhance delivery of nanoparticles, Science, 2013, 339, 971-975.

15. J. Xu, F. He, S. Gai, S. Zhang, L. Li and P. Yang, Nitrogenenriched, double-shelled carbon/layered double hydroxide hollow microspheres for excellent electrochemical performance, Nanoscale, 2014, 6, 10887-10895.

16. N. Ishiguro, S. Kityakarn, O. Sekizawa, T. Uruga, T. Sasabe, K. Nagasawa, T. Yokoyama and M. Tada, Rate enhancements in structural transformations of Pt-Co and Pt-Ni bimetallic cathode catalysts in polymer electrolyte fuel cells studied by in situ time-resolved X-ray absorption fine structure, J. Phys. Chem. C, 2014, 118, 15874.

17. G. Shim, J. Lee, J. Kim, H. J. Lee, Y. B. Kim and Y. K. Oh, Functionalization of nano-graphenes by chimeric peptide engineering, RSC Adv., 2015, 5, 49905-49913.

18. M. E. Lund, J. To, B. A. O'Brien and S. Donnelly, The choice of phorbol 12-myristate 13-acetate differentiation protocol influences the response of Thp-1 macrophages to a proinflammatory stimulus, J. Immunol. Methods, 2016, 430, 64-70.

19. O. A. Timofeeva, et al., Mechanisms of unphosphorylated Stat3 transcription factor binding to DNA, J. Biol. Chem., 2012, 287, 14192-14200.

20. N. G. Sosale, T. Rouhiparkouhi, A. M. Bradshaw, R. Dimova, R. Lipowsky and D. E. Discher, Cell rigidity and shape override Cd47's "self"-signaling in phagocytosis by hyperactivating myosin-II, Blood, 2015, 125, 542-552.

21. J. Gabrielsson and D. Weiner, Non-compartmental analysis, Methods Mol. Biol., 2012, 929, 377-389.

22. W. Miao, G. Shim, S. Lee and Y. K. Oh, Structure-dependent photothermal anticancer effects of carbon-based photoresponsive nanomaterials, Biomaterials, 2014, 35, 4058-4065.

23. T. M. Allen and P. R. Cullis, Liposomal drug delivery systems: from concept to clinical applications, Adv. Drug Delivery Rev., 2013, 65, 36-48.

24. H. Y. Wu, K. J. Lin, P. Y. Wang, C. W. Lin, H. W. Yang, C. C. Ma, Y. J. Lu and T. R. Jan, Polyethylene glycol-coated graphene oxide attenuates antigen-specific IgE production and enhanced antigen-induced T-cell reactivity in ovalbumin-sensitized Balb/C mice, Int. J. Nanomed., 2014, 9, 4257.

25. M. J. Feito, M. Vila, M. C. Matesanz, J. Linares, G. Goncalves, P. A. Marques, M. Vallet-Regı´, J. M. Rojo and M. T. Portole´s, In vitro evaluation of graphene oxide nanosheets on immune function, J. Colloid Interface Sci., 2014, 432, 221-228.

26. H. Hatakeyama, H. Akita and H. Harashima, A multifunctional envelope type nano device (MEND) for gene delivery to tumours based on the EPR effect: a strategy for overcoming the PEG dilemma, Adv. Drug Delivery Rev., 2011, 63, 152-160.

27. H. Hatakeyama, H. Akita and H. Harashima, The polyethyleneglycol dilemma: advantage and disadvantage of PEGylation of liposomes for systemic genes and nucleic acids delivery to tumors, Biol. Pharm. Bull., 2013, 36, 892-899.

28. H. Okazawa, S. Motegi, N. Ohyama, H. Ohnishi, T. Tomizawa, Y. Kaneko, P. A. Oldenborg, O. Ishikawa and T. Matozaki, Negative regulation of phagocytosis in macrophages by the CD47-SHPS-1 system, J. Immunol., 2005, 174, 2004-2011.

29. J. A. Swanson, Shaping cups into phagosomes and macro-pinosomes, Nat. Rev. Mol. Cell Biol., 2008, 9, 639-649.

30. M. G. Kim, J. Y. Park, Y. Shon, G. Kim, G. Shim and Y. K. Oh, Nanotechnology and vaccine development, Asian J. Pharm. Sci., 2014, 9, 227-235.

31. J. Y. Park, M. G. Kim, G. Shim and Y. K. Oh, Lipid-based antigen delivery systems, J. Pharm. Invest., 2016, 46, 295-304.

32. R. P. Garay, R. El-Gewely, J. K. Armstrong, G. Garratty and P. Richette, Antibodies against polyethylene glycol in healthy subjects and in patients treated with PEG-conjugated agents, Expert Opin. Drug Delivery, 2012, 9, 1319-1323.

33. C. Lubich, et al., The mystery of antibodies against polyethylene glycol (PEG)- What do we Know?, Pharm. Res., 2016, 33, 2239-2249.

34. M. Ichihara, T. Shimizu, A. Imoto, Y. Hashiguchi, Y. Uehara, T. Ishida and H. Kiwada, Anti-PEG IgM response against PEGylated liposomes in mice and rats, Pharmaceutics, 2011, 3, 1-11.

35. S. Sunoqrot, J. Bugno, D. Lantvit, J. E. Burdette and S. Hong, Prolonged blood circulation and enhanced tumor accumulation of folate-targeted dendrimer-polymer hybrid nanoparticles, J. Controlled Release, 2014, 191, 115-122.

36. M. O. Durymanov, A. A. Rosenkranz and A. S. Sobolev, Current approaches for improving intratumoral accumulation and distribution of nanomedicines, Theranostics, 2015, 5, 1007-1020.

37. M. P. Chao, I. L. Weissman and R. Majeti, The CD47-SIRPα pathway in cancer immune evasion and potential therapeutic implications, Curr. Opin. Immunol., 2012, 24, 225-232.

38. A. D. Garg, E. Romano, N. Rufo and P. Agostinis, Immunogenic versus tolerogenic phagocytosis during anticancer therapy: mechanisms and clinical translation, Cell Death Differ., 2016, 23, 938-951.

국문초록

펩타이드 수식 그래핀을 이용한 혈중 지속시간 증강연구

박규태
약학과 물리약학전공
서울대학교

본 연구에서는 대식세포의 포식작용을 억제하는 기작을 갖는 종양세포표면의 단백질인 분화클러스터 47(Cluster of Differentiation 47; CD47)을 모방한 펩타이드(CD47-like SIRPα-binding peptide; SP)로 표면을 수식한 그래핀옥사이드(Graphene oxide; GO)나노시트를 소개하고 있다. 공초점현미경을 통해 폴리에틸렌글리콜(Polyethylene glycol; PEG)로 수식한 GO나노시트와 SP-GO나노시트의 *in vitro* 인간 대식세포 내 유입을 실험한 결과, SP-GO나노시트 처리그룹에서 포식 작용의 현저한 감소를 확인할 수 있었다. SCC7종양이 형성된 마우스에 정맥 주사한 후 약물 동태학적 매개변수와 종양조직 분포율을 측정한 결과, PEG-GO나노시트보다 SP-GO나노시트의 혈중 지속시간과 종양주위 형광 강도가 유의한 수준으로 높았다. 이러한 결과들로 긴 생체지속성과 높은 종양조직분포율을 가지는 펩타이드 수식 그래핀이 향후 항암제나 조영제 등을 탑재하는 등 다방면의 바이오의약시스템에 응용될 수 있음을 제시하였다.

주요어 : 펩타이드, 그래핀 나노시트, 생체지속성, 대식세포, 포식작용
학 번 : 2016-21833